Environ Fluid Mech (2017) 17:1081–1098
DOI 10.1007/s10652-017-9536-x

ORIGINAL ARTICLE

Dimensionless numbers for classifying the thermodynamics regimes that determine water temperature in shallow lakes and wetlands

Alberto de la Fuente[1] · **Carolina Meruane**[1,2]

Received: 17 June 2016 / Accepted: 10 May 2017 / Published online: 16 May 2017

Abstract The influence of sediments in the heat budget of water bodies has been reported to be determinant in shallow lakes and wetlands, whereas it is usually neglected in larger water bodies. In this article, we address the question of whether or not sediments should be considered in the computation of water temperature, by defining two dimensionless numbers that describe the thermodynamics regimes of shallow lakes and wetlands. These dimensionless numbers rise from the analysis of the role of periodic heat exchanges at the sediment–water interface (SWI) on the water temperature of shallow lakes and wetlands. The analysis was based on the derivation of an analytic solution that adopts the solution for the second Stokes problem for computing the sediment temperature, when the system is forced by periodic (diurnal, seasonal, decadal) heat exchanges with the atmosphere. The first dimensionless number is the ratio between the thermal inertia of the active sediments and the thermal inertia of the water column, and quantifies the role of sediments on the heat budget. The second dimensionless number, on the other hand, is defined as the ratio between the timescale of changes in the external forcing and the timescale required to reach the heat equilibrium at the SWI, and characterizes the influence of turbulence on the water column on heat exchanges across the SWI. We complemented the analysis with field observations conducted in shallow lakes of 5–15 cm depth, whose thermodynamics is controlled by heat exchanges between the water column and the sediments. As the dimensionless numbers defined here are frequency dependent, we show that one particular process can be neglected for one specific frequency, while it cannot be neglected for other frequencies. In the case of lakes and deep wetlands, sediments could be neglected in a diurnal time-scale, while they should be included for seasonal or decadal time-scales. The relevance of this frequency-dependence is that it suggests that sediments should always be considered in long-term climatic simulations.

✉ Alberto de la Fuente
aldelafu@ing.uchile.cl

[1] Departamento de Ingeniería Civil, Universidad de Chile, Santiago, Chile

[2] Modelación Ambiental SpA., Santiago, Chile

Keywords Thermodynamics model · Shallow lakes · Dimensionless numbers · Wetlands · Water–sediment heat flux

1 Introduction

The mixing and vertical transport processes operating on lakes are well known [11]. In these systems, the major features of the thermodynamics regimes are assessed by computing the values of the Richardson, Wedderburn and Lake numbers, which have been used for classifying thermodynamic regimes of these systems [12, 21, 24]. However, in the case of shallow lakes and wetlands, it is still difficult to determine the thermodynamics regimes, mainly because water temperature is not only modulated by heat exchanges with the atmosphere, but also with the bottom sediments [3]. In this article, we attempt to provide an analogous approach for classifying thermodynamics regimes that determine water temperature in shallow lakes and wetlands, which are based on dimensionless numbers presented and discussed in this article.

Water temperature is a key parameter that controls the dynamics of the aquatic ecosystems, as it defines, among many other factors, primary production and respiration rates, biochemical reactions rates; and controls vertical transports in stratified water bodies [27]. Several factors control water temperature of water bodies, including heat exchanges with the atmosphere and sediments, inflows and outflows, internal heating due to penetrative solar radiation and buoyancy. Particularly, water depth controls the thermodynamics of water bodies as it defines the influence of thermal inertial in the heat budget [7]. For extremely shallow waters of a few centimeter depths, however, heat inertia is small enough, such as water temperature is primarily modulated by heat exchanges with the atmosphere as well as sediments. In this sense, de la Fuente and Niño [4] showed that heat exchanges at the water–sediment interface are keys to understand water temperature as they reduce the amplitude of dial oscillation in the water temperature, by capturing or releasing heat during day and night, respectively. Heat diffusion in the sediments is responsible for this heat reservoir role of the sediments [3]. Furthermore, de la Fuente [3] showed that for shallow lakes, surface sediments absorb solar radiations in a thin layer whose thickness depends on light penetration properties of the surface sediments. As a consequence, temperature shows maximum values right below the sediment–water interface (SWI), and this excess of heat either diffuses toward the water column or deeper sediments. As the temperature is maximum near the SWI, convective conditions are also associated, thus enhancing mechanical heat transport from the sediments to the water column [3]. Similar dynamics has been observed in shallow rivers [10]. In contrast, for deeper lakes, sediments temperature tend to an equilibrium value equal to the annual mean temperature in deep areas of the lake, whereas the amplitude of the seasonal oscillation at the water–sediment interface depends on both the size of the lake and light penetration depth or maximum water depth, depending on which one is the smallest [6]. This is because the sediments temperature is defined by water temperature, without any feedback [6]. As a result, the adiabatic boundary condition is usually considered in lakes, thus neglecting the influence of sediments in the thermodynamics of the water body [9, 22]. However, a formal analysis for determining under which circumstances heat exchanges with the sediments can be neglected is missing. Particularly, it is not clear when the heat diffusion at the SWI is dominated by either the sediment-side, the water-side of the SWI, or

both. In order to assess this thermodynamics behavior, dimensionless numbers are required.

The objective of this article is to study the role of periodic heat exchanges at the water–sediment interface on the water temperature of shallow lakes and wetlands. This analysis is conducted based on an analytic solution presented here for computing water and sediments temperature, and this solution allows for identifying two dimensionless numbers that describe the thermodynamics of shallow lakes and wetlands. The first dimensionless number quantifies the role of sediments in the heat budget, while the second one characterizes the influence of turbulence in the waterside of the SWI on heat exchanges across the SWI. The combination of both dimensionless numbers allows determining whether or not bottom sediments participate on the water heat budget.

This article is organized as follows. In the Methods section, we describe the governing equations and present the analytic solution for the problem, which is formulated in terms of a Fourier expansion of the heat flux at the air–water interface (AWI). Consequently, water temperature is written in terms of periodic functions, and the solution of the Second problem of Stokes can be adopted for sediment temperature. The Second problem of Stokes solves the diffusion equation given a periodic Dirichlet boundary condition and a Neumann (adiabatic) boundary condition in the infinite [1]. This spectral approach is detailed starting from a simple case without a heat-reservoir function of the sediments. We then consider the following complex cases: with a heat-reservoir function of the sediments, and with feedback between the water temperature and heat fluxes exchanged with the atmosphere. Finally, we list the algorithm for the full model, which includes all the processes. In the Results section, we follow the same order described in the Methods section, proving simple computational examples and the validation of the model against field observations in a shallow lake. Finally, in the last section we discuss de results and show that the analytic solution allowed for identifying two dimensionless numbers that quantify the importance of sediments (Π_1), and heat transfer velocity (Π_2) in the water temperature of shallow waters.

2 Methods

2.1 Governing equations

The vertically integrated heat conservation equation for a water column of height h with a vertically homogeneous water temperature T_w is written as follows [3, 10, 16, 17],

$$(\rho c_p)_w h \frac{\partial T_w}{\partial t} = H + H_g \tag{1}$$

where $(\rho c_p)_w$ is the heat capacity of the water ($(\rho c_p)_w \approx 4.4 \times 10^6$ J $(\mathrm{m}^3\ \mathrm{K})^{-1}$) and H (Wm^{-2}) is the heat flux exchanged across the air–water interface (AWI) such that $H > 0$ represents the heat flux from the atmosphere to the water [2, 8]. H denotes the net heat fluxes exchanged with the atmosphere, thus including net short wave radiation (incident minus reflected), net long wave radiation (incident minus emitted), and the latent and sensible turbulent heat fluxes [8, 25]. Finally, H_g is the heat flux exchange at the water–sediment interface (SWI) such that $H_g > 0$ represents the heat flux from the sediments to the water column.

H_g can be either computed from the sediment-side of the SWI (at $z = 0^-$) or the water-side of the SWI. From the sediment-side, H_g can be evaluated as

$$H_g = -\kappa_s \left(\rho c_p\right)_s \left.\frac{\partial T_s}{\partial z}\right|_{z=0^-} \tag{2}$$

where κ_s is the thermal diffusion coefficient in the sediments (between 0.01 and 0.11 $m^2\ day^{-1}$, [6, 20]), $(\rho c_p)_s$ denotes the heat capacity of the sediments (between 1.4 and 3.8×10^6 J $(m^3\ K)^{-1}$ [6, 20], and T_s is the sediment temperature that varies in space (z) and time. T_s is obtained from the heat diffusion equation in the sediments [20, 23], written as

$$\frac{\partial T_s}{\partial t} = \kappa_s \frac{\partial^2 T_s}{\partial z^2} \tag{3}$$

Equation 3 is solved with heat flux and temperature continuity at the SWI, and the adiabatic boundary condition is required at $z = -\infty$.

From the water-side of the SWI (at $z = 0^+$), H_g can be calculated as

$$H_g(t) = -k_t \left(\rho c_p\right)_w (T_w - T_{WSI}) \tag{4}$$

where T_{WSI} is the temperature at the SWI and k_t is the heat transfer velocity that depends on the bottom shear velocity and/or heat convection [13, 15, 18]. Flux and temperature continuity at the SWI implies that H_g calculated with Eq. (2) is equal to H_g calculated with Eq. 4, where $T_{WSI} = T_s(z = 0^-)$.

2.2 Water temperature in shallow waters for $H_g = 0$

In order to introduce the basis for understanding the role of periodic heat exchanges at the SWI in natural shallow water, we first consider the simple case where $H_g = 0$ and H is a discrete function that can be expanded as a Fourier series of $2N + 1$ terms as

$$H = \sum_{n=-N}^{N} H_n e^{i\omega_n t} \tag{5}$$

where $i = \sqrt{-1}$, $\omega_n = 2\pi n/\Delta t(2N + 1)$ is the frequency of the *nth* term of the Fourier expansion, and Δt is the time step of the temporal discretization of H. The coefficients H_n can be obtained using a fast Fourier transform (*fft*) of H. In particular, if $Y = fft(H)$, the *nth* amplitude H_n is computed as $H_n = Y_n/(2N + 1)$. Then, the water temperature is expanded in a Fourier expansion of $2N + 1$ terms as

$$T_W(t) = \sum_{n=-N}^{N} T_{wn} e^{i\omega_n t} \tag{6}$$

where T_{wn} are the temperature amplitudes of the expansion. These temperature amplitudes of the expansions are constant and are the unknowns of the problem. Then, Eq. 6 is replaced in Eq. 1, which provides

$$\sum_{n=-N}^{N} i\Omega_n T_{wn} e^{i\omega_n t} = \sum_{n=-N}^{N} H_n e^{i\omega_n t} \tag{7}$$

where $\Omega_n = \omega_n h(\rho c_p)_w$. Finally, for $n \neq 0$, the solution for the temperature amplitudes is written as

$$T_{wn} = -i\frac{H_n}{\Omega_n} \tag{8}$$

The solution for $n = 0$ is discussed in the subsection "Influence of T_w on H". Furthermore, Eq. 8 provides a temperature scale T^*_{wn} defined as

$$T^*_{wn} = \frac{H_n}{\Omega_n} \tag{9}$$

which represents the thermal amplitude that can be reached in the absence of sediments.

2.3 Water temperature in shallow waters for $H_g \neq 0$

For including the heat exchanged with the sediment in the previous solution, the temperature at the SWI is also expanded into a Fourier series, as

$$T_{WSI} = \sum_{n=-N}^{N} T_{sn} e^{i\omega_n t} \tag{10}$$

where T_{sn} are the SWI temperature amplitudes of the nth term of the expansion. The temperature at the SWI is the boundary condition for the heat diffusion linear equation in the sediments (Eq. 3). As a consequence, the sediment temperature can also be expanded in a series of solutions such that each one of them is the solution of the well-known Stokes' second problem, which describes the solution of the diffusion equation forced by a periodic Dirichlet function in a semi-infinite domain [1, 20]. Considering this, the sediment temperature can be written as

$$T_s(z,t) = \sum_{n=-N}^{N} T_{sn} e^{i\omega_n t} e^{(1+s_n i)\alpha_n z} \tag{11}$$

where $\alpha_n = \sqrt{abs(\omega_n)/2\kappa_s}$ is the inverse of the length scale of heat penetration into the sediments (see [1], and s_n is the sign of n. Then, Eq. 2 can be directly evaluated for obtaining

$$H_g = -\kappa_s(\rho c_p)_s \sum_{n=-N}^{N} \alpha_n T_{sn} e^{i\omega_n t}(1 + s_n i) \tag{12}$$

Similarly, for the water-side of the SWI, Eq. 4 can be written as:

$$H_g = -k_t(\rho c_p)_w \sum_{n=-N}^{N} (T_{wn} - T_{sn}) e^{i\omega_n t} \tag{13}$$

Two cases are identified. The first case considers the turbulent transport in the water-side of the SWI to be very efficient (i.e., $k_t = +\infty$) such that $T_{WSI} = T_w$ and H_g is determined using Eq. 12 with $T_{sn} = T_{wn}$. As a consequence, Eq. 1 can be written as

$$\sum_{n=-N}^{N} i\Omega_n T_{wn} e^{i\omega_n t} = \sum_{n=-N}^{N} H_n e^{i\omega_n t} - \sum_{n=-N}^{N} \kappa_s \left(\rho c_p\right)_s \alpha_n T_{wn} e^{i\omega_n t}(1 + s_n i) \tag{14}$$

which result in T_{wn} for $n \neq 0$ being written as

$$T_{wn} = \frac{H_n}{(i\Omega_n + (1 + s_n i)D_n)} \tag{15}$$

where $D_n = (\rho c_s)_s k_s \alpha_n$. The value of T_{wn} for $n = 0$ is described in detail in the following subsection. Based on this result, a first dimensionless number is identified as

$$\Pi_1 = \frac{D_n}{\Omega_n} = \frac{(\rho c_s)_s}{\left(\rho c_p\right)_w} \frac{1}{2h\alpha_n} \tag{16}$$

Π_1 is a dimensionless number that accounts for the influence of sediments on the heat budget of the water column h. Π_1 can be understood as the ratio between the thermal inertia of the active sediments of thickness $1/\alpha_n$ and the thermal inertia of the water column of depth h ($(\rho c_s)_w h$). Accordingly to values used by Fang and Stefan [6], the ratio $(\rho c_s)_s/(\rho c_p)_w$ takes values between 0.32 and 0.86 for sediment composition between sandy sediments to organic materials. With the definition of Π_1 and the temperature scale T^*_{wn}, Eq. 15 can be written as

$$\frac{T_{wn}}{T^*_{wn}} = \frac{1}{(i + (1 + s_n i)\Pi_1)} \tag{17}$$

An interesting limit to this case is when $h = 0$ such as the heat flux exchanged with the atmosphere is balanced by ground heat flux [8]. This balance provides

$$T_{wn} = \frac{H_n}{(1 + s_n i)D_n} \tag{18}$$

where a second temperature scale can be defined as $T^{*s}_{wn} = H_n/D_n$, which is the temperature amplitude that is obtained in the absence of a water column, thus representing amplitude of land surface temperature.

In the second case, $T_{WSI} \neq T_w$, and therefore, the rate of diffusion across the thermal boundary layer in the water should be considered for computing H_g. Similar to the previous cases, the solution for $n \neq 0$ is written as:

$$T_{sn} = \frac{K}{K + (1 + is_n)D_n} T_{wn} \tag{19}$$

and

$$T_{wn} = H_n \left(i\Omega_n + K\left(1 - \frac{K}{K + (1 + is_n)D_n}\right)\right)^{-1} \tag{20}$$

where $K = k_t \left(\rho c_p\right)_w$. A second dimensionless number is defined as:

$$\Pi_2 = \frac{K}{\Omega_n} = \frac{k_t}{\omega_n h} \tag{21}$$

which quantifies the influence of turbulent transport in the water column on H_g. Π_2 can be understood as the ratio between the timescale associated to changes in the external forcing (ω_n^{-1}) and the timescale required to reach the heat equilibrium at the SWI (h/k_t), described by $T_w = T_s$.

Finally, Eqs. 19 and 20 can be written in a dimensionless form as

$$\frac{T_{sn}}{T_{wn}} = \frac{\Pi_2}{\Pi_2 + (1 + is_n)\Pi_1} \tag{22}$$

and

$$\frac{T_{wn}}{T_{wn}^*} = \left(i + \Pi_2 \left(1 - \frac{\Pi_2}{\Pi_2 + (1 + is_n)\Pi_1} \right) \right)^{-1} \tag{23}$$

2.4 Influence of T_w on H

So far, we have adopted an explicit method where H is independent of computed water temperature, which is not correct. Consequently, the implicit influence of T_w on H is included by linearizing H in a similar way than it is done for the finite volume method [19, 26], such that

$$H = \alpha_H - \beta_H T_w \tag{24}$$

where α_H is a time series and β_H should be a positive constant value. With this linearization of the source term, the time series α_H is expanded into a Fourier series as

$$\alpha_H = \sum_{n=-N}^{N} H_n^{\alpha} e^{i\omega_n t} \tag{25}$$

Following this, H is written as

$$H = \sum_{n=-N}^{N} \left(H_n^{\alpha} - \beta_H T_{wn} \right) e^{i\omega_n t} \tag{26}$$

that after replacing in Eq. 1, provides

$$T_{wn} = \frac{H_n^{\alpha}}{\Omega_n} \left(i + \Pi_2 \left(1 - \frac{\Pi_2}{\Pi_2 + (1 + is_n)\Pi_1} \right) + \beta_H \right)^{-1} \tag{27}$$

for $-N \leq n \leq N$, including $n = 0$, where Eq. 27 is reduced to:

$$T_{w0} = \frac{H_0^{\alpha}}{\beta_H} \tag{28}$$

The linearization of the source term H is a standard numerical technique used in implicit iterative schemes such as the finite volume methods [19, 26]. In the context of the spectral formulation presented here, the linearization of H enables us to include the nonlinear dependence of H as a function of T_w, in the context of the linear model behind the Fourier

decomposition of the solution. Furthermore, this implicit formulation of H also enables to include feedback between the water temperature and H. This last aspect provides a solution for the $n = 0$ term of the Fourier decomposition, also called the zero-frequency term of the spectral model. This is observed in Eq. 14 where both the heat inertia and the sediment diffusion terms are equal to 0 for $n = 0$. Therefore, Eq. 14 has a solution for $n = 0$ only if the frequency independent term of the Fourier decomposition of H is zero. The physical interpretation of this requirement is that the average net heat flux exchanged with the atmosphere should be zero ($H_o = 0$ of Eq. 5), and this heat balance at the AWI is allowed to be achieved by enabling to H to self-adjust as a function of T_w. In this way, the average incident heat flux is balanced by an average heat flux from the water to the atmosphere, whose magnitude grows with the water temperature (long wave radiation, evaporation and/or convection). This average heat balance is reached by linearizing H such that Eq. 14 for $n = 0$ is written to $H_0^\alpha - \beta_H T_{w0} = 0$.

2.5 Full model

The full model for computing T_w for non-idealized cases is detailed as follows. The iterative algorithm considers the following: (1) H is a nonlinear function of T_w and is computed by considering atmospheric boundary layer stability with the parameterizations used in the Kansas experiments [8, 12]. (2) k_t varies within the day and may also be driven by convection [3, 5, 18]; however, a constant characteristic value of k_t (k_t^*) is required for the spectral model. The value of k_t^* required for computing K is also updated at any iteration. Finally, (3) the iteration starts with a constant water temperature $T_w^{(0)} = 10°C$. Given these assumptions, for the iteration $k + 1$, the algorithm is described as follows:

1. Compute H as a function of $T_w^{(k)}$(herein after called H^*); and use it to compute α_H and β_H required to linearize the heat flux exchanged with the atmosphere of Eq. 24. Here, α_H and β_H are obtained with a first order Taylor expansion to express $H^{(k+1)}$ in the form of Eq. 24, as a function of $H^*, T_w^{(k+1)}$ and $T_w^{(k)}$. It is obtained that

$$H^{(k+1)} = H^* - \beta_H \left(T_w^{(k+1)} - T_w^{(k)} \right) \tag{29}$$

with

$$\beta_H = -avg\left(\frac{\partial H}{\partial T_w} \right) \approx -avg\left(\frac{\left(H\left(T_w^* + \varepsilon \right) - H\left(T_w^* \right) \right)}{\epsilon} \right) \tag{30}$$

where $avg(\cdot)$ is the average of the argument and ϵ is a small value of the order 10^{-5}. Following this definition of Eq. 29 it is obtained that

$$\alpha_H = H^* + \beta_H T_w^{(k)} \tag{31}$$

Furthermore, Eq. 29 shows that if the convergence of the model is good ($T_w^{(k+1)} \approx T_w^{(k)}$), then $H^{(k+1)} \approx H^*$, which means that the forcing heat exchanges with the atmosphere is fully dependent on the water temperature, since H^* is a nonlinear function of T_w that includes all the heat fluxes exchanged with the atmosphere. Furthermore, as is shown in the results section, β_H takes values between 10 and 100 $\mathrm{Wm^{-2}\ °C^{-1}}$, and the solution of T_w is not sensible to this parameter.
2. Compute H_n^α of Eq. 25 using a Fourier transform of α_H. In particular, if $Y = fft(\alpha_H)$, then $H_n^\alpha = Y_n/(2N + 1)$.

3. Compute T_{wn} and T_{sn} using Eqs. 19 and 27.
4. Compute the water temperature for the iteration $k+1$, $T_w^{(k+1)}$ (Eq. 6). This can be performed with the inverse Fourier transform (*ifft*) of T_{wn}. In particular, $T_w = ifft(T_{wn})(2N+1)$. However, to increase the convergence of the solution, the use of an under-relaxation factor, r, is recommended, so that $T_w^{(k+1)}$ is finally computed as

$$T_w^{(k+1)} = (1-r)ifft(T_{wn})(2N+1) + rT_w^{(k)} \tag{32}$$

   $r = 0.7$ was used in this article.
5. Update k_t and K. The time series of the wind shear velocity, T_w and T_{WSI} are used for computing one time series of k_t; however, the spectral model requires a constant value of K. The characteristic heat transfer velocity, k_t^*, can be either the average k_t ($k_t^* = avg(k_t)$) or

$$\frac{1}{k_t^*} = avg\left(\frac{1}{k_t}\right) \tag{33}$$

   which enhances the influence of small values of k_t on the characteristic transfer velocity. Here $avg(\cdot)$ denotes the average function of the argument. The influence of this assumption is discussed in the following section.
6. Check the convergence of the solution, and return to step 1 if required. Here we used the maximum absolute difference between $T_w^{(k+1)}$ and $T_w^{(k)}$ to check the convergence of the model, and a threshold value of 10^{-4} °C to stop the simulation.

2.6 Field observations

Field measurements in Salar del Huasco (Fig. 1a) recorded by de la Fuente [3] were used to validate the spectral model for computing the water temperature in shallow wetlands. Detailed information is available for the period between the evening of the 29th of October and noon of the 31st of October of 2012 presented by de la Fuente [3]. This information includes water temperature and meteorological information at the point marked with a filled white circle in Fig. 1a. We considered a water depth $h = 5$ cm. The thermodynamic model is detailed in de la Fuente [3], who showed that the bulk albedo for the wetland is 0.17, and the heat exchanges across the SWI and the AWI are dominated by both heat convection during calm conditions (Fig. 1b) and wind shear stress during windy conditions in the afternoons (Fig. 1c).

3 Results

3.1 Dimensionless numbers

To investigate the role of dimensions numbers Π_1 (Eq. 16) and Π_2 (Eq. 21) in the solution of T_w, a simple case was analyzed where H is a monochromatic function depicted in Fig. 2a, written as:

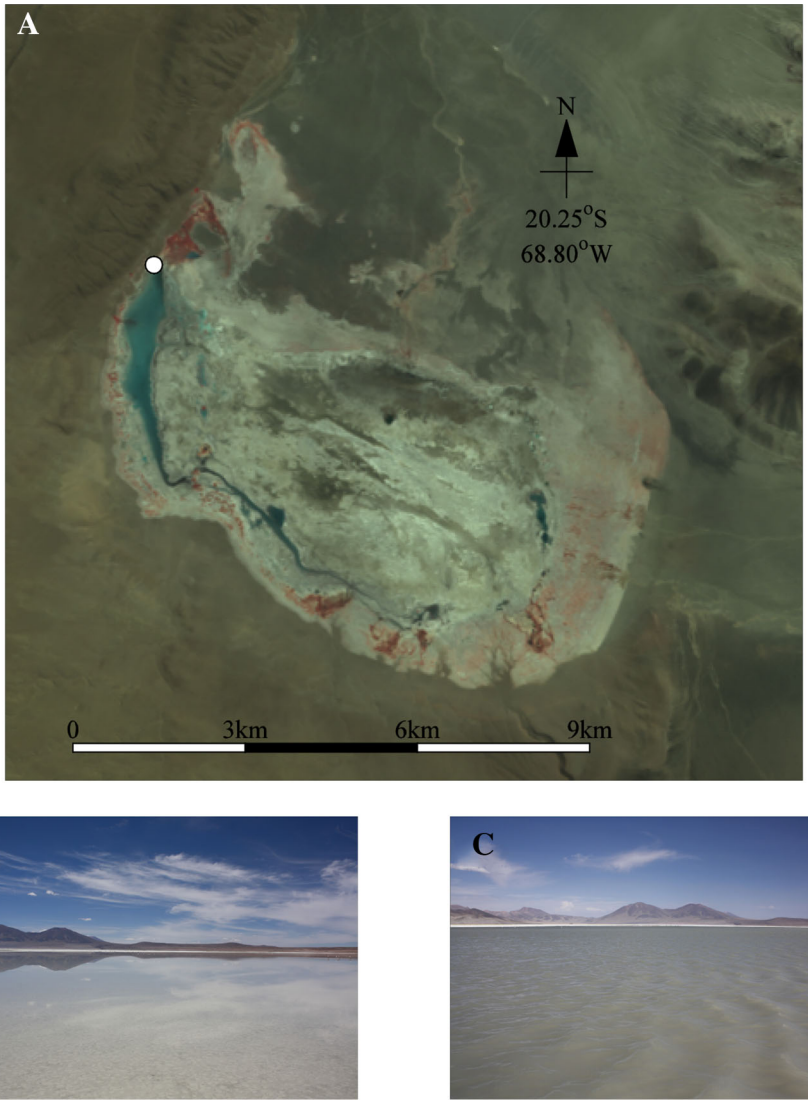

Fig. 1 **a** Satellite image of Salar del Huasco, and location of the meteorological stations installed in October 2012 (*filled white circle*). **b**, **c** Picture of Salar del Huasco during calm and windy conditions, respectively

$$H = \Delta H \cos \omega_k t = \frac{\Delta H}{2}\left(e^{i\omega_k t} + e^{-i\omega_k t}\right) \tag{34}$$

Figure 2a shows the time series of H, while Fig. 2b shows the time series of T_w for the case $H_g = 0$, which in this case is given by (see Eq. (8) with $n = \pm 1$).

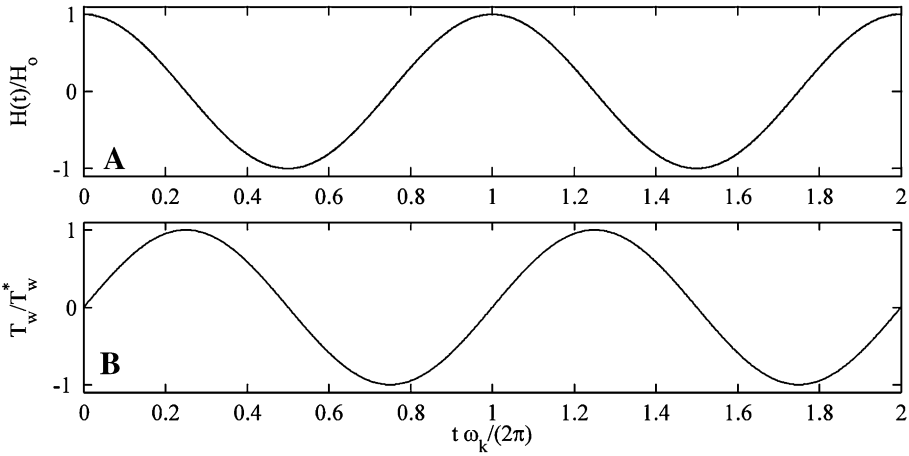

Fig. 2 **a** Time series of the monochromatic heat flux exchanged with the atmosphere, and **b** time series of the water temperature computed for the simple case $H_g = 0$

$$T_w = -i\frac{\Delta H}{2\Omega_k}\left(e^{i\omega_k t} - e^{-i\omega_k t}\right) = \frac{\Delta H}{\Omega_k}\sin\omega_k t \tag{35}$$

Equation 35 shows that in the absence of sediments, the water temperature reaches a maximum at a fourth of the period of forcing after the maximum H value is reached.

With respect to the influence of the first dimensionless number Π_1, Fig. 3 shows the effect of including H_g in the computation of T_w for the limiting case $k_t \to \infty$. The time series of H is shown in Fig. 3a, while Fig. 3b, c show the time series of the water temperature and H_g for the extreme values $\Pi_1 = 0$ (dashed line) and $\Pi_1 = \infty$ (solid line). Figure 3d shows the maximum value of H_g as a function of Π_1. The limit $\Pi_1 = 0$ represents the case when there is no heat storage in the sediments ($H_g = 0$). This limit is equivalent to deep water bodies or fast frequencies. On the contrary, as Π_1 increases, the influence of H_g in the heat budget increases as the limit $H_g = H$ is achieved when $\Pi_1 \to \infty$. This limit is represented by cases with $h \to 0$ described by Eq. 18 or for low frequencies of days and years. From a practical point of view, Fig. 3d suggest that for $\Pi_1 \gtrsim 10$, the water column is shallow enough such that the heat storage in the water column can be neglected, and T_{WSI} is obtained by solving $H_g = H$ (solid line in Fig. 3b, c).

Finally, the role of the dimensionless parameter Π_2 is shown in Fig. 4, where $\Pi_1 = 1$. The value $\Pi_2 = 0$ represents the limit where no heat exchanges occurs across the SWI because $k_t = 0$. Therefore, the solution is described using Eq. 35 (see the dashed lines in Fig. 4b, c). On the contrary, when $\Pi_2 \to \infty$, the turbulent transport in the water column is energetic enough such that H_g is controlled by heat transport in the sediment-side of the SWI. From a practical point of view, this limit occurs for $\Pi_2 \gtrsim 5$. In the context of the definition of Π_2 as the ratio between the timescale of changes in the external forcing and the timescale required to reach the heat equilibrium at the WSI, large values of Π_2 mean that the equilibrium $T_s = T_w$ is quickly reached in the context of temporal changes in H. On the contrary, if changes in the external forcing occur faster than the timescale required to reach the heat equilibrium at the SWI, Π_2 is small and values of k_t turns to be relevant in the dynamics.

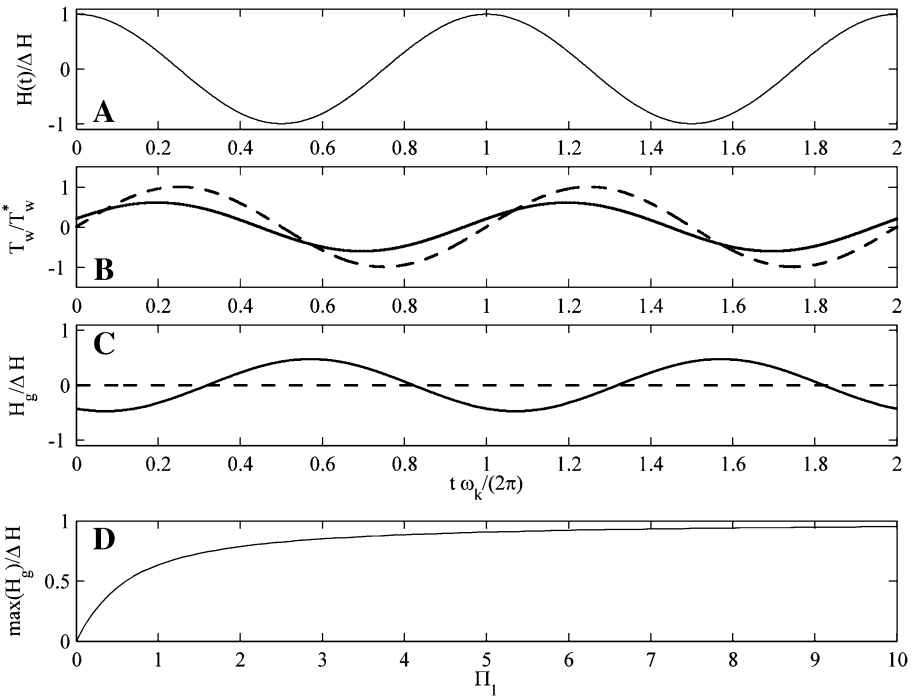

Fig. 3 **a** Time series of the monochromatic heat flux exchanged with the atmosphere. **b** Time series of the water temperature computed for the limits $\Pi_1 = 0$ (*dashed line*) and $\Pi_1 = \infty$ (*solid line*). **c** Similar to (**b**), for the time series of H_g. **d** Influence of Π_1 on the maximum value of H_g

3.2 On the influence of k_t in H_g

Meteorological data and water temperature measured in Salar del Huasco in October of 2012 were used to estimate β_H. Based on these measurements, Fig. 5a shows the time series and $-\partial H/\partial T_w$ computed using Eq. 30 and the measured T_w is plotted in Fig. 5b. It is observed that the coefficient β_H ranges between 5 and 70 $\mathrm{Wm^{-2}\ ^\circ C^{-1}}$, with an average of $\beta_H = 21.7\ \mathrm{Wm^{-2}\ ^\circ C^{-1}}$. Because of the influence of latent and sensible turbulent heat fluxes at the AWI, $-\partial H/\partial T_w$ is proportional to the wind shear velocity (Fig. 5c). The dashed lines in Fig. 5a show three characteristic values of $-\partial H/\partial T_w$ that are used as β_H in the following calculus (5, 20 and 60 $\mathrm{Wm^{-2}\ ^\circ C^{-1}}$).

Figure 6a shows the observed (grey thick line) and the simulated T_w with the spectral model for $\beta_H = 20\ \mathrm{Wm^{-2}\ ^\circ C^{-1}}$, and $k_t^* = avg(k_t)$ (solid black line) and k_t^* of Eq. 33 (dashed black line) as the characteristic heat transfer velocity. The time-series of T_w shown in Fig. 6a was constructed in 50 iterations, and the convergence of the solutions shows that for iteration 50, the difference between $T_w^{(k+1)}$ and $T_w^{(k)}$ was approximately 10^{-5} °C (Fig. 7b) in both simulations with $k_t^* = avg(k_t)$ (grey circles) and k_t^* of Eq. 33 (white triangles). In Fig. 6b, $\delta T_w = abs\left(T_w^{(k+1)} - T_w^{(k)}\right)$. As the convergence of the model was good, the influence of β_H in the computation of T_w can be neglected for reasonable values of this parameter. The maximum value of the absolute difference between T_w computed for the different β_H considered was approximately 10^{-4} °C.

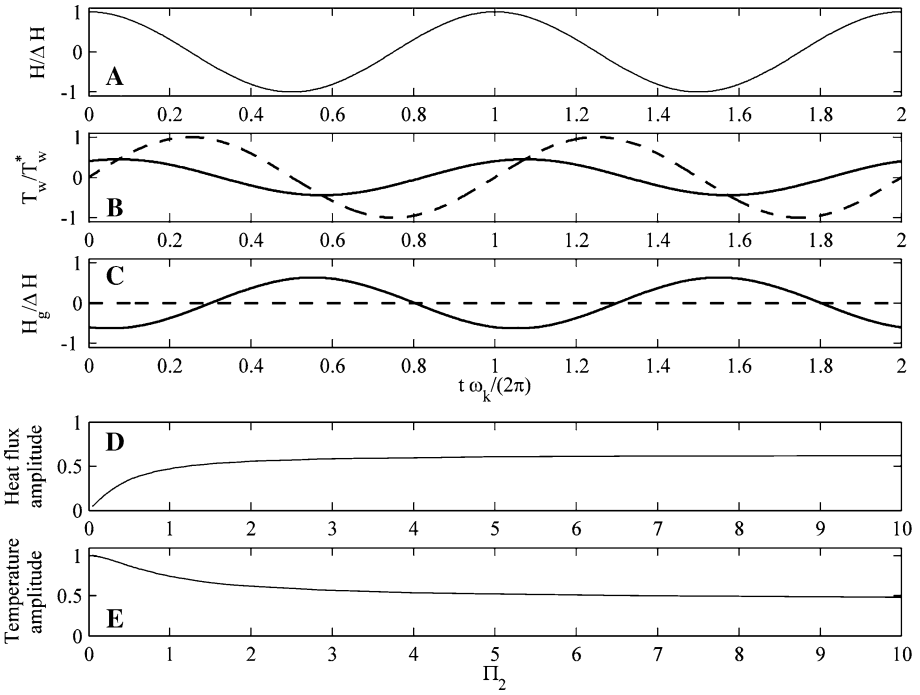

Fig. 4 **a** Time series of the monochromatic heat flux exchanged with the atmosphere. **b** Time series of the water temperature computed for $\Pi_1 = 1$ and the limits $\Pi_2 = 0$ (*dashed line*) and $\Pi_2 = \infty$ (*solid line*). **c** Similar to (**b**), for the time series of H_g. **d** Influence of Π_2 on the maximum value of H_g. **e** Similar to (**d**), for the temperature amplitude

Dimensionless numbers identified based on the spectral model showed that the water temperature is influenced by heat exchanges with the sediments; however, the heat transfer velocity in the water-side is large enough, so that H_g is not influenced by the value of k_t. The first conclusion was obtained by examining the value of T_{wn} as a function of Π_1, as shown in Fig. 7a. According to this plot, larger complex amplitudes are associated with $\Pi_1 \approx 1$. According to Fig. 3d, $\Pi_1 \approx 1$ indicates that heat exchanges with the sediments constitute approximately 60% of the heat exchanges with the atmosphere. To prove the second conclusion (the value of k_t is large enough such that H_g is controlled by the sediment-side of the SWI), two simulations were carried out with k_t^* given by Eq. 33 (grey line in Fig. 7b) and $k_t^* = avg(k_t)$ (dashed line in Fig. 7b). The simulated water temperature is not sensitive to the value of k_t^*, and the reason for this response is that larger complex amplitudes (T_{wn}) are associated with values of $\Pi_2 > 2$ (see Fig. 7c). According to Fig. 4d, this range of Π_2 is associated with H_g larger than 88% of the value that is obtained when considering $k_t^* = +\infty$ (Fig. 3). Furthermore, the independence of water temperature on the value of k_t is more relevant for larger periods associated to small values of ω_k, which has associated larger values of $\Pi_2 = k_t/\omega_k h$.

Finally, to quantify the error associated to the linearization of H, required to reach a solution for the zero-frequency terms of the spectral decomposition, Fig. 8 shows in grey color the time series of H computed for $\beta_H = 20$ Wm^{-2} °C^{-1} and the final water temperature denoted as T_w^{k+1} after 50 iterations (grey area). Furthermore, Fig. 8 plots the time

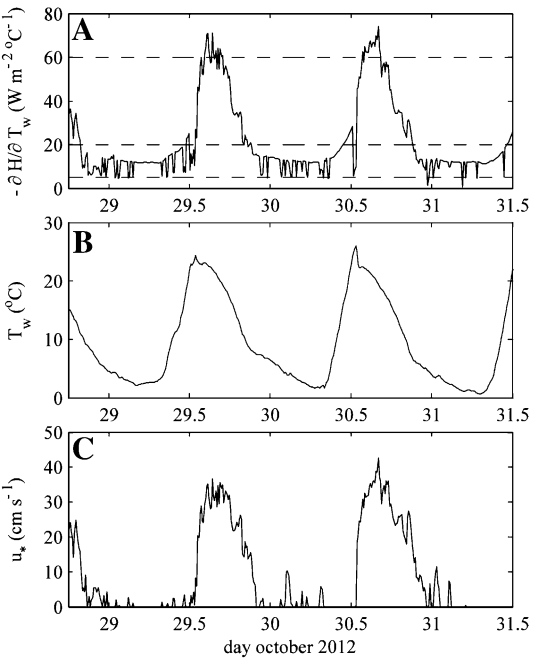

Fig. 5 **a** Computed time series of $-\partial H/\partial T_w$(*solid line*) and the values of $\beta_H = 5$, 20 and 60 $\mathrm{Wm}^{-2}\ ^{\circ}\mathrm{C}^{-1}$ used for the simulation (*dashed line*). **b** Measured time series of the water temperature in Salar del Huasco in October 2012. **c** Measured time series of the wind shear velocity in Salar del Huasco in October 2012

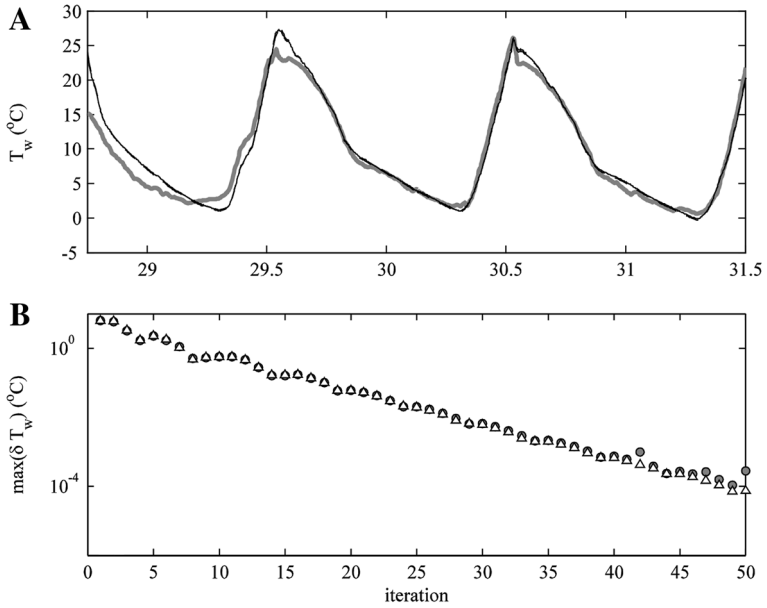

Fig. 6 **a** Comparison between the observed water temperature (*grey thick line*) and simulated water temperature and the spectral model with $\beta_H = 20\ \mathrm{Wm}^{-2}\ ^{\circ}\mathrm{C}^{-1}$; and $k_t^* = avg(k_t)$ (*black solid line*) and k_t^* computed using Eq. (33) (*dashed*). *Black solid* and *dashed lines* are overlapped. **b** Evolution of the error of the spectral model as a function of the number of iterations

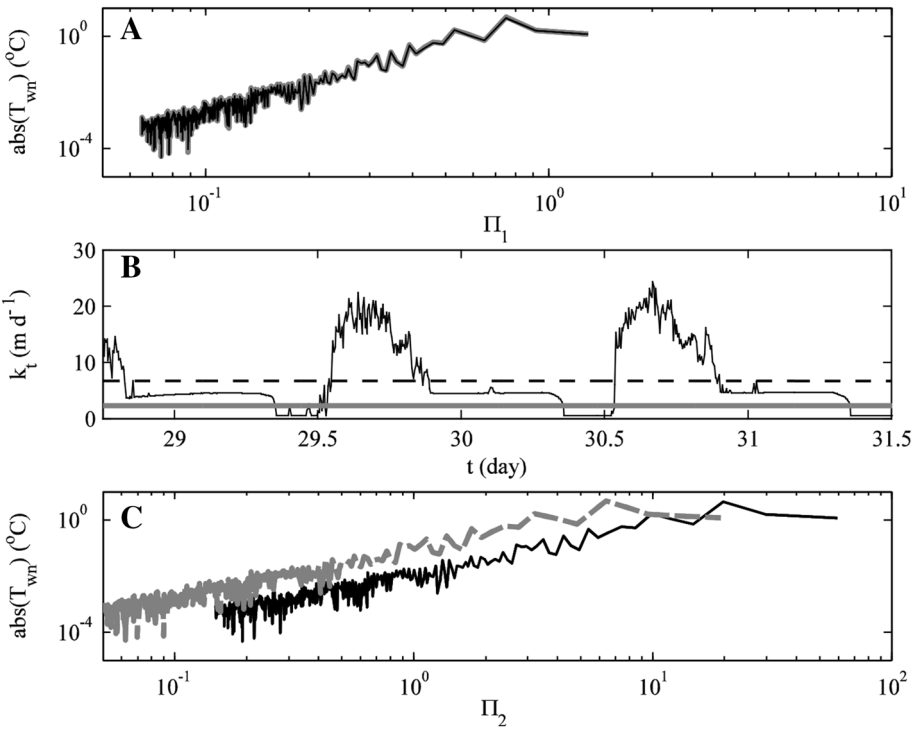

Fig. 7 **a** Absolute value of the temperature amplitude T_{wn} as a function of Π_1 for simulation with $k_t^* = avg(k_t)$ (*black line*) and k_t^* computed using Eq. (33) (*grey line*). **b** Time series of k_t (*solid black line*), $k_t^* = avg(k_t)$ (*dashed line*), and k_t^* computed using Eq. (26) (*grey line*). **c** Absolute value of the temperature amplitude T_{wn} as a function of Π_2 for simulation with $k_t^* = avg(k_t)$ (*black line*) and k_t^* computed using Eq. (33) (*grey line*)

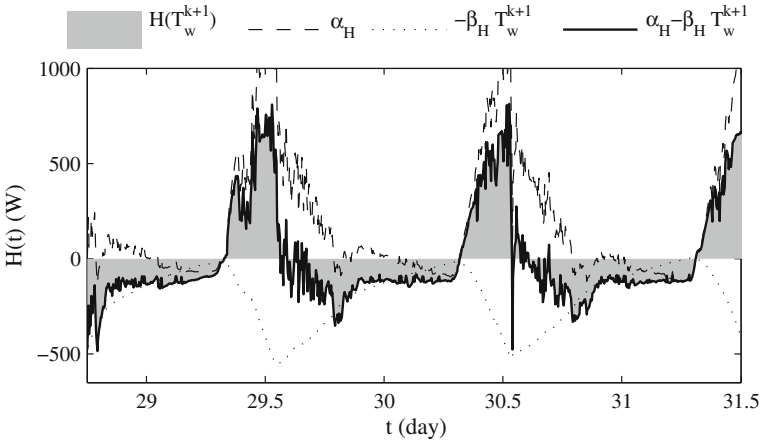

Fig. 8 Time series of H computed with the simulated T_w after 50 iterations and $\beta_H = 20\ \mathrm{Wm}^{-2}\ \mathrm{K}^{-1}$ (*grey area*), and the corresponding time series of α_H (*dashed line*), $-\beta_H T_w^{k+1}$ (*dotted line*) and $H^{(k+1)} = \alpha_H - \beta_H T_w^{k+1}$ (*solid line*)

series of α_H, $-\beta_H T_w^{k+1}$ and the linearized heat flux exchanged with the atmosphere $H^{(k+1)} = \alpha_H - \beta_H T_w^{k+1}$. The time series of $H^{(k+1)}$ estimated by linearizing H matches very well with the fully nonlinear time series of H computed with T_w^{k+1}, and square root difference between both time series is equal to 0.002 Wm^{-2}. This result is not sensitive on the value of β_H. As a consequence, to linearize H provides a solution for the zero-frequency temperature, and the resulting time series of H fully captures the nonlinear dependence of H on the water temperature.

4 Discussion

In this article we have derived an analytic solution for the water temperature in shallow systems forced by periodic (diurnal, seasonal, decadal) heat exchanges with the atmosphere. This analytic solution allowed for identifying two dimensionless numbers that quantify the importance of sediments (Π_1) and heat transfer velocity (Π_2) in the water temperature of shallow waters.

The dimensionless number Π_1 quantifies the importance of sediments, and Fig. 3 shows that the influence of H_g on water temperature increases with Π_1. Larger values of Π_1 are achieved for low frequencies. This result is concordant with that of Fang and Stefan [6], who showed that the initial condition for the temperature of deep sediments (approximately 10 m) is required for computing the water temperature in long-term simulations spanning two decades. In the context of the spectral model, no initial condition was required, and this is because the model computes the temperature amplitudes of the expansion rather than the temperature at one particular time step.

The limitations of this spectral approach are related to the fact that k_t, κ_s, $\left(\rho c_p\right)_s$ and $\left(\rho c_p\right)_w$ should be constants. Although this assumption can be reasonable for molecular properties κ_s, $\left(\rho c_p\right)_s$ and $\left(\rho c_p\right)_w$, assuming that a constant k_t can be used to reproduce heat exchanges between the water and sediment requires further justification (see Fig. 7). This justification was made based on the second dimensionless number, Π_2, which was defined based on the formulation of the spectral model. This dimensionless number was defined to quantify the influence of k_t on H_g in such a way that if $\Pi_2 = k_t/\omega_k h > 5$, k_t is large enough, so that H_g is conditioned by the heat diffusion in the sediment and not by turbulent diffusion in the water column. By definition, Π_2 is inversely proportional to the frequency, which allow us to conclude that the value of k_t is important only for high frequencies that explains changes in water temperature in the hourly time-scale. In fact, the results presented in Fig. 7 show that the value of k_t is not relevant for the dominant waves that characterize the diurnal cycles ($\omega_n = 2\pi/12$ hr and $2\pi/24$ hr). However, it is important to notice that Π_2 decreases as h increases; thus, the value of k_t should be important in deeper water bodies.

The dimensionless numbers defined here are frequency dependent, and the question whether a process is relevant or not depends on the particular frequency that is studied. For example, the importance of heat fluxes exchanged with the sediments is expected to occur for large values of Π_1, which occurs in shallow lakes at small frequencies. Consequently, sediments can be neglected in one particular time-scale (diurnal time-scale), while they should be included for other frequencies (seasonal or decadal time-scales). The relevance of this frequency-dependence is that it suggests that sediments should be considered in

climatic simulations [14], although they can perfectly be neglected in the diurnal or seasonal time-scales.

Furthermore, the use of the solution for computing water temperature in extremely shallow lakes of the Altiplano region of South America, confirm previous studies that showed that heat exchange between the water and the sediments plays an important role in the heat budget of water column [3, 4]. However, we were also able to show that for the dominant periods of 12 and 24 h, this heat flux is not determined by the heat transfer velocity k_t. With respect to the application to shallow lakes of the Altiplano, de la Fuente [3] also showed that for the measurements used in this article, 53% of the short wave solar radiation is absorbed in the water column and 29% of the downward shortwave solar radiation is absorbed in the top layer of the sediments, thus explaining overheated conditions below the SWI. However, the spectral model presented here is not able to differentiate between heat absorbed in the water column and heat absorbed in the sediments, and simply considered that 83% of the downward solar radiation is absorbed in the water column (i.e., albedo of 0.17). However, as de la Fuente [3] also pointed out, to not differentiate between these two pathways for absorption of shortwave solar radiation produces a small error in the simulated water temperature.

5 Conclusion

The thermodynamics regimes in lakes are well described by dimensionless numbers; however, in the case of shallow lakes and wetlands, it is still difficult to determine the thermodynamics regimes, mainly because water temperature is not only modulated by heat exchanges with the atmosphere, but also with the bottom sediments. In this contribution, we provided an analogous methodology based on two dimensionless numbers, for classifying the thermodynamics regimes that determine water temperature in shallow lakes and wetlands.

The first dimensionless number, Π_1, was defined in Eq. 16, and accounts for the influence of sediments on the heat budget of the water column h. Π_1 is understood as the ratio between the thermal inertia of the active sediments and the thermal inertia of the water column of depth h. The active sediments in the thermodynamic context are located near the SWI, and their temperature varies accordingly to changes in the water temperature. The thickness of this active layer depends on the frequency of the forcing such that a seasonal cycle has a thicker active layer than diurnal cycle.

The second dimensionless number, Π_2, was defined in Eq. 21, and quantifies the influence of turbulent transport in the water column on H_g. Π_2 is proportional to the heat transfer velocity, and Fig. 4 showed that turbulent transport across the SWI is important only when it is weak ($\Pi_2 \lesssim 2$) with respect to diffusion in the sediment-side of the SWI.

Acknowledgements This study was financed by the Fondecyt project number 1140821.

References

1. Batchelor GK (1967) An introduction to fluid dynamics. Cambridge University Press, Cambridge
2. Bogan T, Mohsemi O, Stefan HG (2003) Stream temperature-equilibrium temperature relationship. Water Resour Res 39:1243

3. de la Fuente A (2014) Heat and dissolved oxygen exchanges between the sediment and water column in a shallow salty lagoon. J Geophys Res Biogeosciences 119:596–613
4. de la Fuente A, Niño Y (2010) Temporal and spatial features of the thermohydrodynamics of shallow salty lagoons in northern Chile. Limnol Oceanogr 55:279–288. doi:10.4319/lo.2010.55.1.0279
5. de la Fuente A, Ordóñez C, Pérez R (2016) Diffusional mass transfer coefficient at the water–sediment interface for wind-induced flow in very shallow lagoons. Environ Fluid Mech 16:539–558. doi:10.1007/s10652-015-9437-9
6. Fang X, Stefan HG (1998) Temperature variability in lake sediments. Water Resour Res 34:717–729
7. Fischer H, List R, Imberger J, Brooks N (1979) Mixing in island and coastal waters. Academic Press, London
8. Garratt JR (1992) The atmospheric boundary layer. Cambridge University Press, Cambridge
9. Hipsey MR, Sivapalan M, Clement TP (2004) A numerical and field investigation of surface heat fluxes from small wind-sheltered waterbodies in semi-arid Western Australia. Environ Fluid Mech 4:79–106. doi:10.1023/A:1025547707198
10. Hondzo M, Stefan HG (1994) Riverbed heat conduction prediction. Water Resour Res 30:1503–1513. doi:10.1029/93WR03508
11. Imberger J (1998) Flux path in a stratified lake: a review. In: Imberger J (ed) Physical processes in Lakes and Oceans. American Geophysical Union, Washington, DC, pp 1–17
12. Imberger J (2013) Environmental fluid dynamics: flow processes, scaling, equations of motion, and solutions to environmental flows. Academic Press, London
13. Le PM, Papavassiliou DV (2006) Turbulent heat transfer in plane couette flow. J Heat Transfer 128:53. doi:10.1115/1.2130404
14. MacKay MD, Neale PJ, Arp CD, De Senerpont Domis LN, Fang X, Gal G, Jöhnk KD, Kirillin G, Lenters JD, Litchman E, MacIntyre S, Marsh P, Melack J, Mooij WM, Peeters F, Quesada A, Schladow SG, Schmid M, Spence C, Stokesr SL (2009) Modeling lakes and reservoirs in the climate system. Limnol Oceanogr 54:2315–2329. doi:10.4319/lo.2009.54.6_part_2.2315
15. Martynenko OG, Khramtsov PP (2005) Free-convective heat transfer: with many photographs of flows and heat exchange. Springer, Berlin
16. McCabe RM, Estrade P, Middleton JH, Melville WK, Roughan M, Lenain L (2010) Temperature variability in a shallow, tidally isolated coral reef lagoon. J Geophys Res 115:C12011. doi:10.1029/2009JC006023
17. McJannet D, Cook F, McGloin R, McGowan H, Burn S, Sherman B (2013) Long-term energy flux measurements over an irrigation water storage using scintillometry. Agric For Meteorol 168:93–107. doi:10.1016/j.agrformet.2012.08.013
18. Necati O (1977) Basic heat transfer. McGraw-Hill, New York
19. Patankar S (1980) Numerical heath transfer and fluid flow. Hemisphere Publishing Corporation, Washington, DC
20. Prats J, Ramos A, Armengol J, Dolz J (2011) Comparison of models for calculation of diel sediment–water heat flux from water temperatures. J Hydraul Eng 137:1135–1147. doi:10.1061/(ASCE)HY.1943-7900.0000434
21. Shintani T, de la Fuente A, Niño Y, Imberger J (2010) Generalizations of the Wedderburn number: parameterizing upwelling in stratified lakes. Limnol Oceanogr 55:1377–1389
22. Silva CP, Marti CL, Imberger J (2014) Horizontal transport, mixing and retention in a large, shallow estuary: Río de la Plata. Environ Fluid Mech 14:1173–1197. doi:10.1007/s10652-013-9330-3
23. Smith NP (2002) Observations and simulations of water–sediment heat exchange in a shallow coastal lagoon. Estuaries 25:483–487. doi:10.1007/BF02695989
24. Spigel R, Imberger J (1980) The classification of mixed-layer dynamics in lakes of small to medium size. J Phys Ocean 10:1104–1121
25. Stull RB (1999) An introduction to boudary layer meteorology. Kluwer Academic Publishers, Dordrecht
26. Versteeg HK, Malalasekera W (1995) An introduction to computational fluid dynamics. The finite volume methods. Longman Group Ltd., Harlow
27. Wetzel RG (2001) Limnology: lake and river ecosystems. Academic Press, London